Supplemental Information

Figure S1. Histopathology reveals extensive tissue architectural restoration during ear regeneration in *Acomys* versus fibrotic scarring in *Mus*, related to Figure 1.

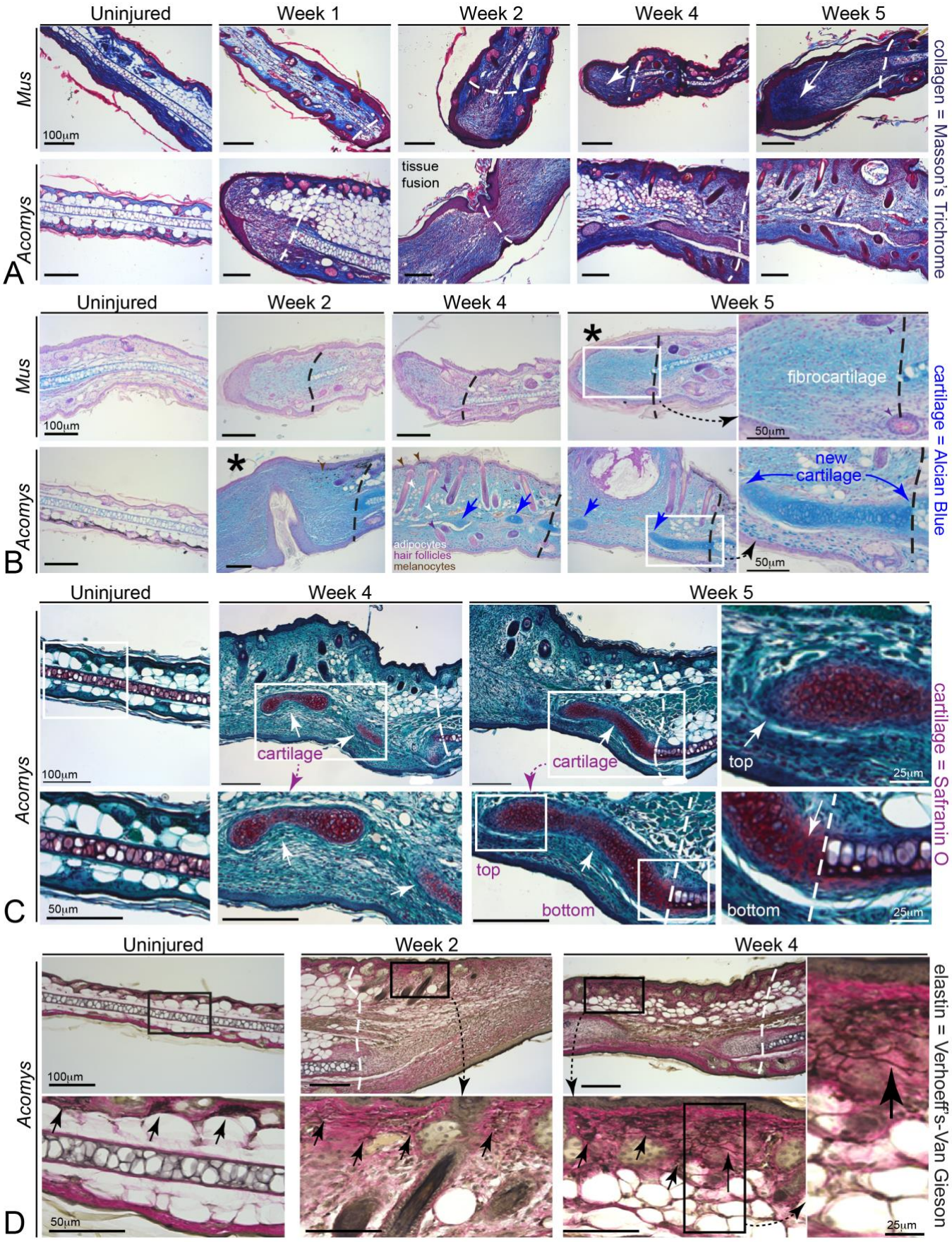

(A) Paraffin sections from *Mus* and *Acomys* timed ear wound series were stained with Masson's Trichome to reveal mature cross-linked collagen (dark blue). Note Mus normally has higher overall levels compared to *Acomys*, forming a distinct and permanent collagen network in the healed subdermal scar (arrows), by contrast to *Acomys* that maintains lower levels at all stages during regenerative healing.

(**B, C**) Similar comparative healing series stained with Alcian Blue (**B**) or Safranin O (**C**) revealed extensive outgrowth of new cartilage from the pre-existing plate and *de novo* formation of cartilage islands within the regenerating tissue by week 4 that continued to mature and structurally organize by week 5: note extensive *de novo* adipocyte formation/differentiation, hair follicle neogenesis, and appearance of new migrating subdermal melanocytes were readily apparent by week 4-5 in *Acomys*. Note also that *Mus* wounds heal/scar with diffuse unstructured fibrocartilage in the subdermal blastema region associated with dense cross-linked collagen (A) without apidocytogenesis or hair follicle neogenesis.

(**D**) *Acomys* adult regeneration includes the re-establishment of long elastin fibers (Verhoeff's-Van Gieson counterstain, brown, arrows) to new tissue architecture near the subdermal region, a process restricted to fetal skin repair in humans (Le Page et al., 2019).

Figure S2. *Acomys* retains *in vivo* regenerative capacity across age and sex, and TGFβ1 signaling induces non-conserved ECM induction in MFs *in vitro*, related to Figure 1.

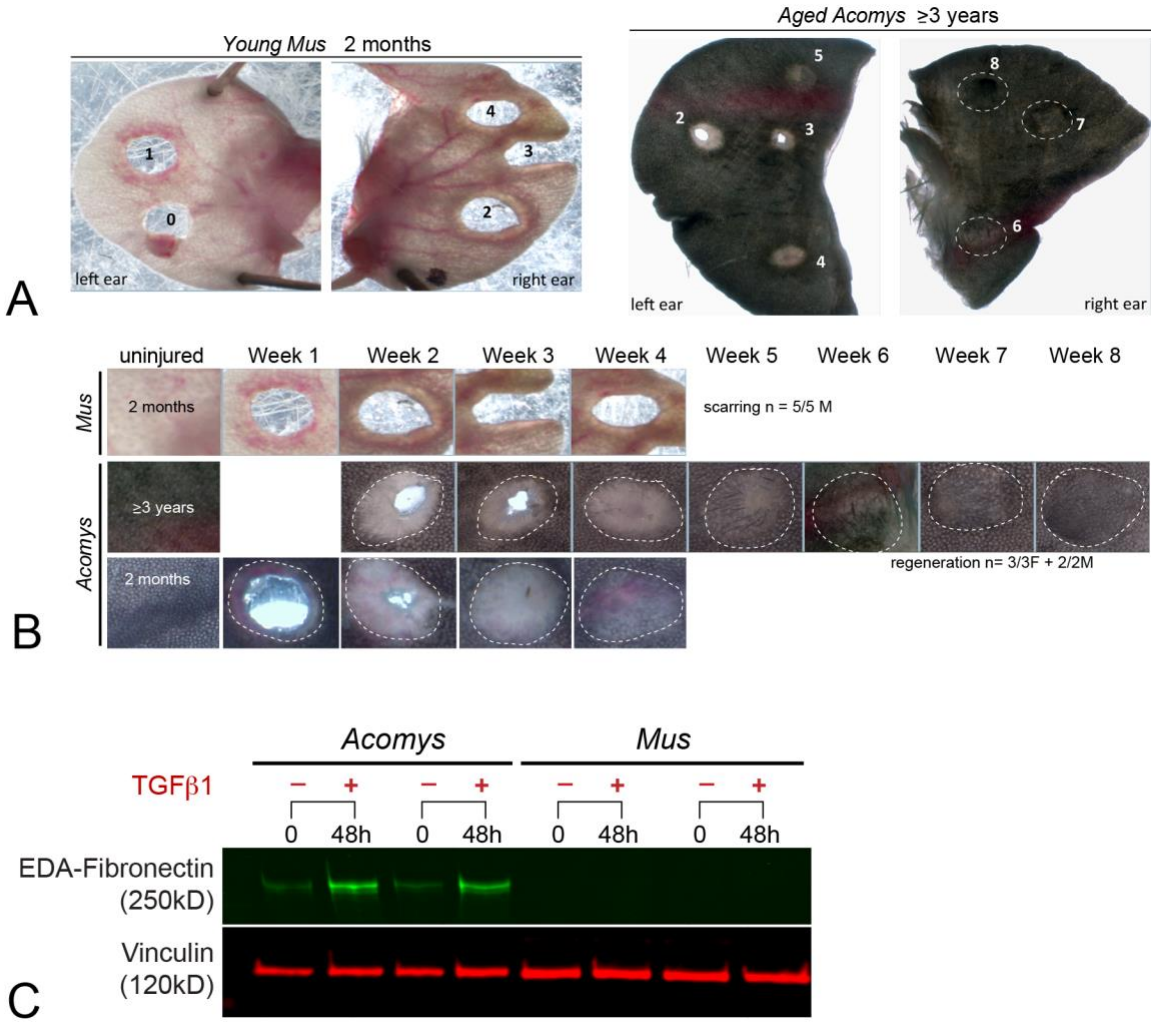

(A) Low-power views of whole ear punch timed injury/healing series between young CD1 Mus (2 months, left) compared to aged Acomys (≥3 years, right).

(**B**) Higher-power views reveal that aged *Acomys* animals from both sexes retain the ability to regenerate multiple 2mm ear punch injuries, including re-pigmentation and hair follicle neogenesis, by contrast to *Mus*: note that regeneration in aged animals may be slightly delayed (~1 week) with respect to young animals (bottom reference panel from **Figure 1A**) but still regenerate.

(**C**) Western blotting revealed Acomys primary ear fibroblasts normally express low levels of EDA-F under control culture conditions that was strongly upregulated after 48h TGFβ1 treatment, by contrast to Mus, indicating operational MF formation *in vitro* as well as *in vivo* (**Figure 1D**) despite non-conserved Acta2 response: independent cultures.

Figure S3. Image analysis pipeline quantification, related to Figure 2 and Figure 5.

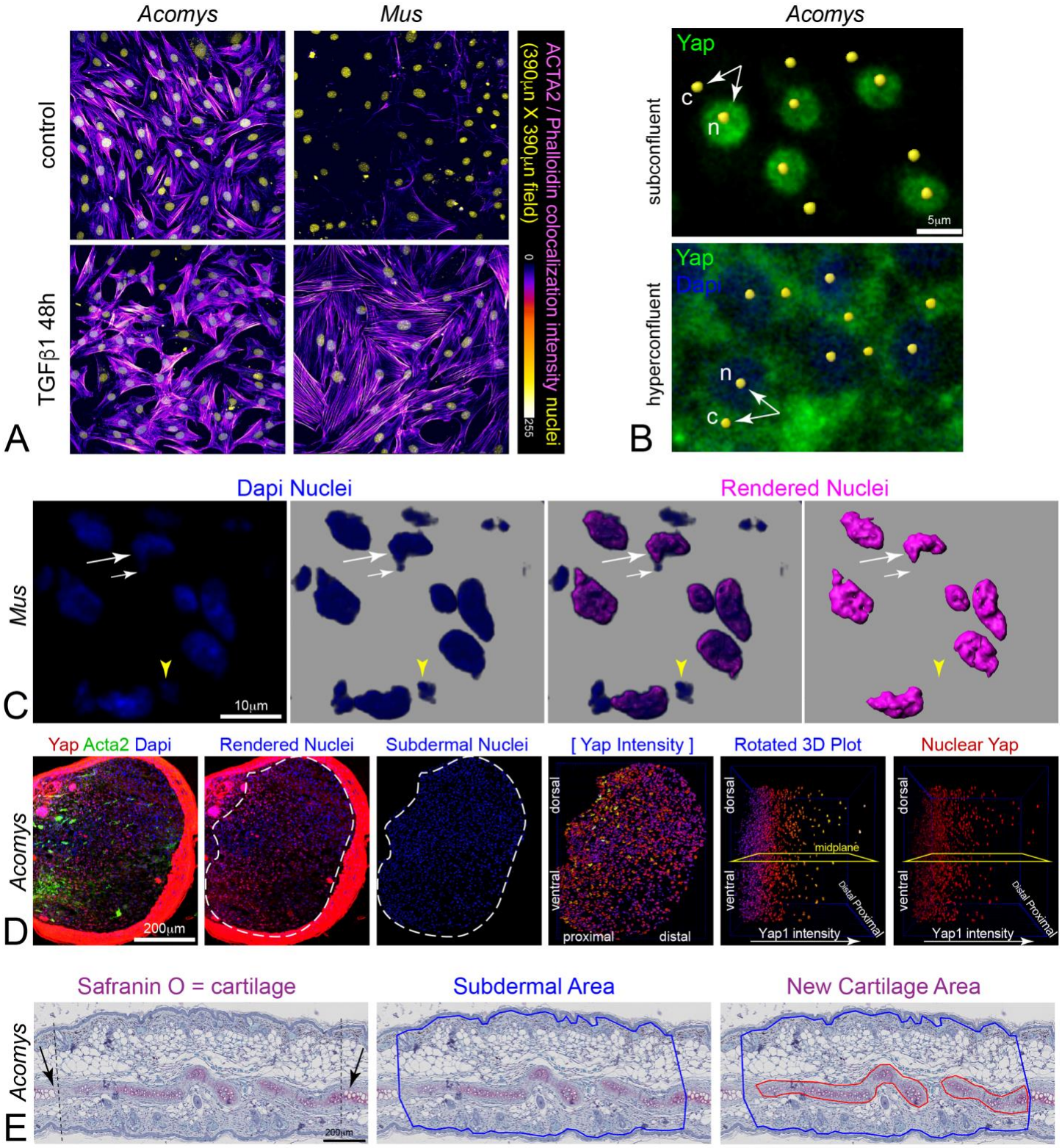

(**A**) Example of *in vitro* Acta2/Phalloidin confocal colocalization channel quantification levels per cell/nuclei field of view.

(**B**) Example of *in vitro* Yap cytoplasmic/nuclear ratios determined by paired 300nm diameter spot analysis of relative Yap intensities (Imaris), with Dapi defined nuclei in 2D images.

(**C**) Example of *in vivo* Yap cytoplasmic/nuclear ratios determined in 3D confocal volumes using Dapi to conservatively render, segment, and filter nuclei.

(**D**) Example of image quantification pipeline for isolating subdermal nuclei, viewing nuclear Yap intensity levels in rotated 3D views to better view dorsal ventral pattern differences.

(**E**) Regenerated cartilage area was determined by quantifying the Safranin O stained new cartilage area within the identified subdermal injury zone.

Figure S4. TGFβ1 induces myofibroblast differentiation in human fibroblast lines, related to Figure 2.

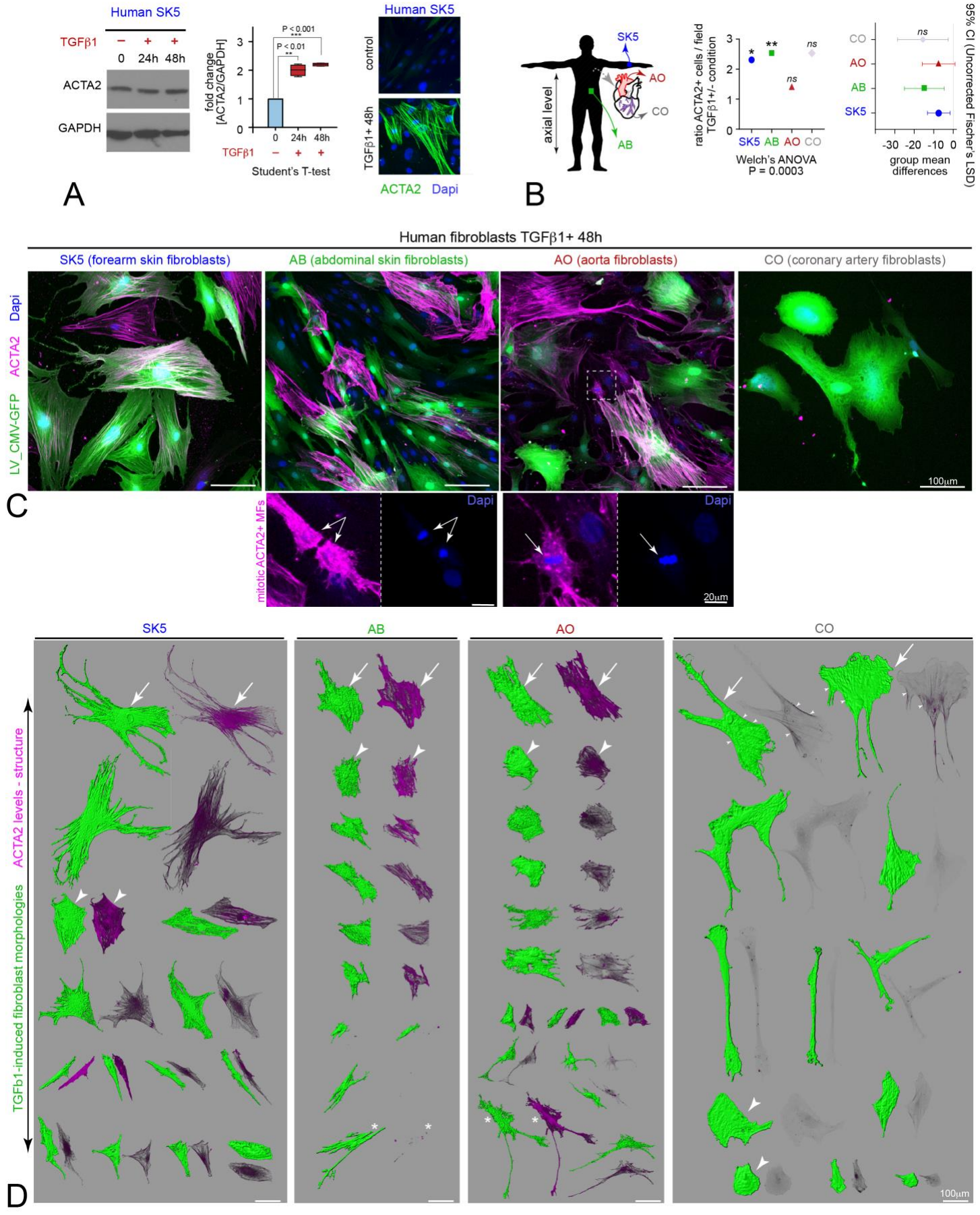

(**A**) Western blot, quantification, and immunofluorescence of human SK5 dermal fibroblasts treated with TGFβ1 compared to controls revealed increased ACTA2 expression and stress fiber formation; data are mean ± SD.

(**B**) Quantification of TGFβ1-mediated ACTA2 immunofluorescence response in additional human fibroblast cell lines from different axial levels and origins: primary abdominal (AB) fibroblasts, aorta (AO) and coronary (CO) vessel fibroblasts: data are ± SD, statistics as indicated, * $P<0.01$, ** $P<0.001$, n.s. and # not significant.

(**C**) Visualization of ACTA2 (magenta) labeling in human TGFβ1-induced MFs in vitro, some of which were transduced with constitutively expressed control GFP lentivirus 2 days prior in order to better visualize complete MF morphologies: note that AB and AO lines were still proliferative after 48h TGFβ1 exposure.

(**D**) Examples of the range of ACTA2 levels and structural organization induced after 48h TGFβ1 exposure; note that large flattened MFs are consistent morphological features in some cells (arrows and arrowheads).

Figure S5. Bioinformatic amino acid sequence of *Acomys* indicates Yap protein is highly conserved in mammals, related to Figure 4.

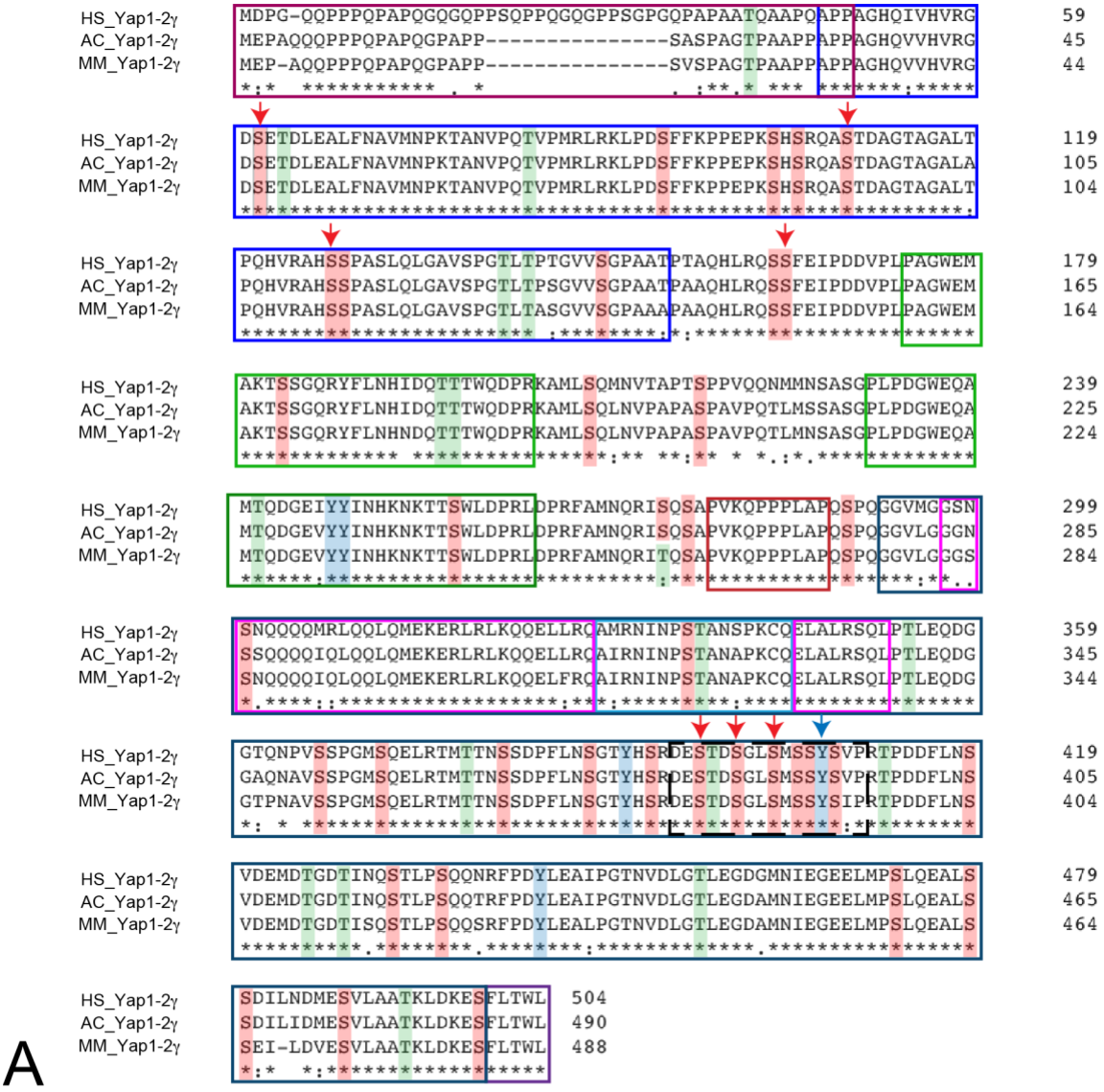

B

Percent Identity

%	HS	AC	MM
HS	100		
AC	93	100	
MM	91	96	100

C

NetPhos 3.1 PO4 prediction

		Acomys	Mus	Human	Conserved
S	Serine	38	39	42	37
T	Theonine	19	19	19	17
Y	Tyrosine	5	5	5	5

(score >0.5, scale 0-1)

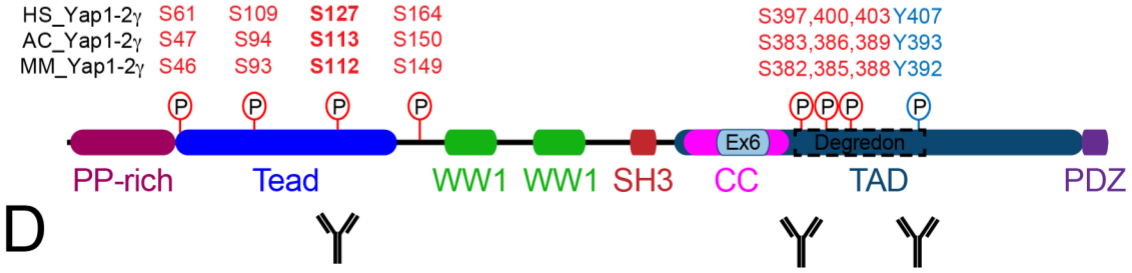

D

(**A**) *Acomys* predicted full-length Yap1 peptide and domain sequence were extracted from our *Acomys cahirinus* Genome (separate publication in prep), and multiply aligned to *Mus* (MM) and human (HS) Yap 1-2γ isoforms using Clustal Omega (www.ebi.ac.uk/Tools/msa/clustalo/), and conserved phosphorylation sites predicted using NetPhos 3.1 (http://www.cbs.dtu.dk/services/NetPhos/) (red arrows indicate Serine phosphorylation sites while blue indicates Tyrosine.

(**B**) Comparison of percent amino acid sequence identity between *A. cahirinus* (AC), *M. musculus* (MM), and human (HS) Yap 1-2 protein.

(**C**) All key conserved sites in human and mouse Yap1 are predicted phosphorylation sites within *Acomys*.

(**D**) Schematic of *Acomys* Yap protein domains compared to known *Mus* and human protein domains, with species-specific AA nomenclature. Antibody cartoons indicate the targeted phosphorylation sites utilized in this study.

Figure S6. Accelerated Yap dephosphorylation kinetics is mediated by a PP2A-class serine/threonine phosphatase in *Acomys* primary ear fibroblasts, related to Figure 4.

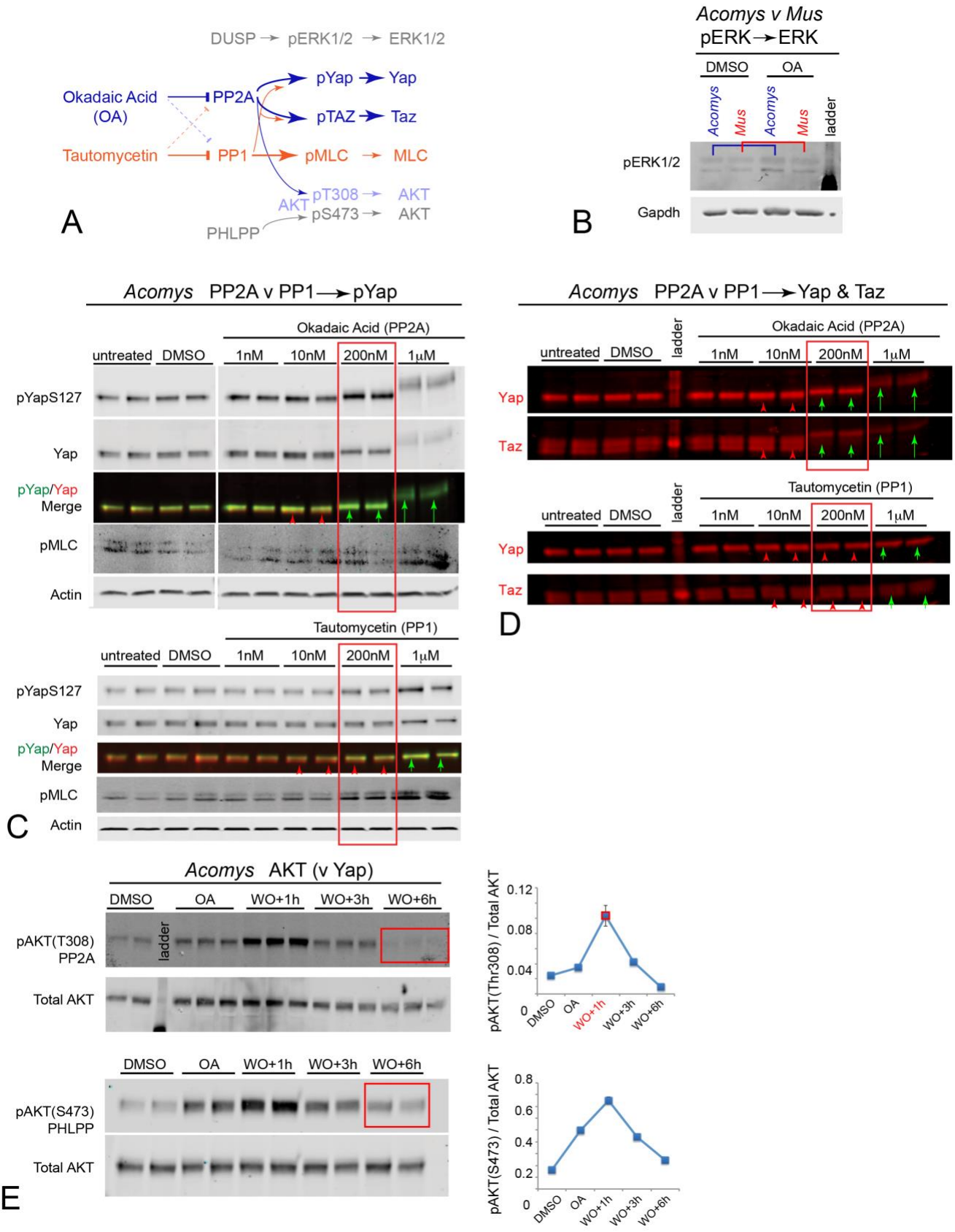

(**A**) Phosphatase substrates and inhibitors used to control for PP2A-mediated rapid Yap dephosphorylation kinetics.

(**B**) Western blots for ERK phosphorylation in *Acomys* versus *Mus* fibroblasts during okadaic acid (OA) pulse show equally low levels of pERK consistent with it being a general DUSP phosphatase substrate (not PP1-PP2A) in both species.

(**C**) Western blots for phosphorylation status of Yap-S127 (pYapS127) and myosin light chain S20 (pMLC) in response to various concentrations of OA, a PP2A-selective inhibitor, compared to tautomycetin, a PP1-selective inhibitor, in *Acomys* dermal fibroblasts (replicate cultures). Selective increases in pYap-S127/total Yap with no change in pMLC levels in the presence of 200nM OA are consistent with a PP2A-class S/T phosphatase activity. Selective increases in pMLC levels with only minor changes in pYap-S127/total Yap at 200nM tautomycetin argue against a major contribution of a PP1-class protein phosphatase activity for pYapS127 in *Acomys*.

(**D**) Independent Western blots confirms bot Yap and Taz are both high-affintiy PP2A substrates compared to PP1, visualized as gel shifts due to increased phosphorylation levels and molecular weights (replicate cultures).

(**E**) Western blots and quantification of phosphorylation status of AKT(T308), a PP2A-dependent substrate (triplicate cultures), compared to AKT(S473), a Phlpp-dependent substrate (replicate cultures), confirms high PP2A phosphatase activity in Acomys fibroblasts: note increased levels of P-T308 at 1h after general WO stress-mediated increase, by contrast to Yap (**Figure 4C,D**), followed by rapid dephosphorylation compared to P-S473 kinetics: data are mean $\pm$ SD.

Figure S7. Comparative *in vivo* YAP signaling patterns and output between *Mus* fibrosis versus *Acomys* regeneration, related to Figure 5 and Figure 6.

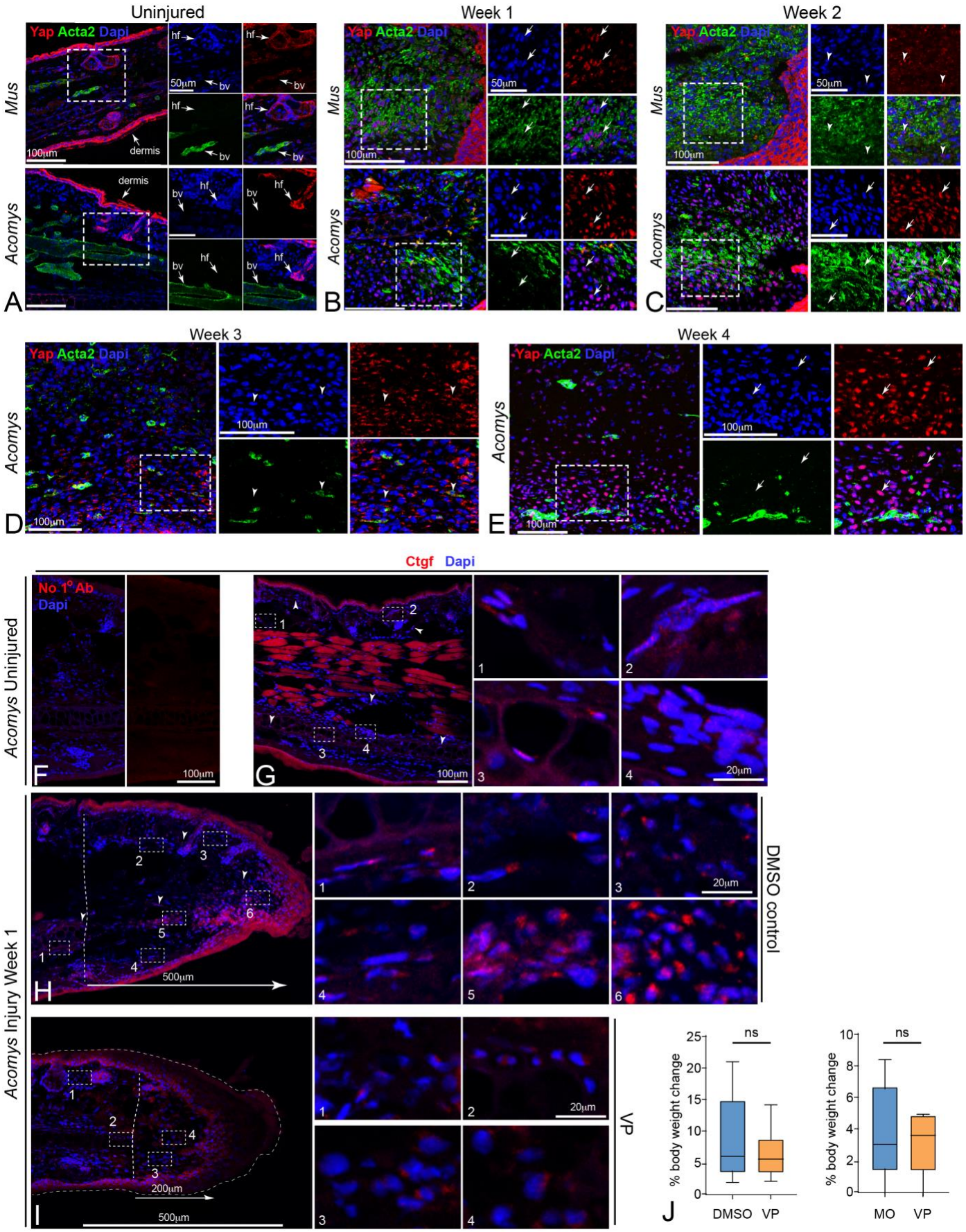

(**A)** Immunostaining for YAP and Acta2 localization in uninjured *Acomys* and *Mus* at indicated time points indicates diffuse Yap cytoplasmic labeling in dermal and subdermal structures with Acta2 localized to BVs (arrows): merged and single-channels. Dashed white boxes indicate areas of higher magnification. Arrows indicate Yap nuclear localization. Arrowheads indicate Yap cytoplasmic localization. BV = blood vessel, HF=hair follicle.

(**B, C**) YAP and Acta2 immunostaining at week 1 (B) and week (2) reveal decreasing perinuclear cytoplasmic Yap localization and levels in $Acta2^{+}$ cells in *Mus* (arrowheads, top panels), by contrast to *Acomys* that exhibit higher nuclear Yap levels (arrows, bottom panels): merged and single-channels.

(**D,E**) *Acomys* Yap labeling re-organizes to the cytoplasm (OFF) at week 3 as tissue closes (**D**), and then switches back to predominately nuclear localization (ON) in many $Acta2^{-}$ cells by week 4, as further patterning and differentiation events continue (**E**), especially in ventral regions.

(**F-J**) *In vivo* validation of the Yap-Tead target Ctgf protein expression, localization, and attenuation due to VP-treatment during *Acomys* regeneration.

(**F**) Uninjured no primary antibody control section imaged at equivalent conditions as sections incubated with anti-Ctgf antibody

(**G-I**) indicates diffuse cytoplasmic labeling in the dermis, and perinuclear labeling in discrete subsets of cells located in the subdermal region, near hair follicles, overlying and within the cartilage plate (**G**, arrowheads and higher power numbered side panels), as well as skeletal muscle fibers, consistent with known sources in *Mus* (Kapoor et al., 2008; Morales et al., 2018).

(**H**) By 1 week of regeneration in *Acomys*, Ctgf expression appears increased in cells in the subdermal blastema and especially near the cartilage plate break, which appear to form a stream migrating outwards into the re-growing tissue underneath the epidermal cap (arrowheads and higher power numbered side panels). (**I**) VP-treatment according to the schedule depicted in **Figure 6A** reveals attenuated outgrowth of new tissue, and decreased Ctgf labeling in cells located in the subdermal region (arrowheads and higher power numbered side panels).

(**J**) Chronic VP-treatment was not overtly toxic: weight change quantification of acute (2 weeks) and chronic (5 weeks) VP (blue) treatment compared to DMSO or MO control (orange): N = ≥4 each group; data are mean $\pm$ SD.

Supplementary Table S1: Top 15 most significantly TGFβ1-induced transcriptional changes in Acomys DFs *in vitro*, related to Figure 2. Top 15 most significantly TGFβ1-induced transcriptional changes in *Acomys* DFs *in vitro*, related to Figure 2 and Supplemental table S2. RNAseq was used to analyze transcriptional responses in *Acomys* primary fibroblasts exposed to low-serum +/- TGFβ1 for 24h (bulk cells, N=3 wells per condition).

Gene (homolog)	logFC	logCPM	PValue adj	FDR
Pai1	**2.647291702**	**5.865759098**	**2.21E-50**	**2.68E-46**
Prg4	2.349346462	4.221240254	3.22E-47	1.95E-43
Sned1	-3.572702583	8.68098451	7.92E-47	3.21E-43
E9Q7P6	2.525836415	6.824202481	2.10E-46	6.38E-43
E9QMD2	2.989355171	9.308402796	2.63E-31	6.38E-28
Tena	2.156944645	7.137936784	1.22E-28	2.47E-25
Atl2	4.450574249	10.63043427	3.12E-27	5.41E-24
Red1	2.552123202	8.523207572	1.36E-26	2.07E-23
Pthd3	-4.079641324	10.58192553	6.41E-26	8.65E-23
Pgh2	2.245182058	8.464638508	1.91E-25	2.32E-22
Ctgf	**1.852407673**	**4.133517831**	**4.40E-23**	**4.85E-20**
CP26A	3.113353436	0.818352124	5.77E-23	5.84E-20
unknown1853	-1.469084857	5.132738894	1.70E-22	1.59E-19
Oasl2	-2.549325574	8.593545338	1.88E-22	1.63E-19
Red = TGFβ1 target *Blue = Yap-Tead target*	FC Fold Change	CPM Counts per Million	Adjusted P value	False Discovery Rate